# DETERMINATION OF REFLECTION COEFFICIENTS BY COMPARISON OF DIRECT AND REFLECTED VSP EVENTS

J.E. LIRA[1], A.B. WEGLEIN[2], C.W. BIRD[3*] and K.A. INNANEN[3]

[1] *Petrobras E&P-Exp/Geof/EGPI, Av. Chile 330, Rio de Janeiro, RJ 20031-170, Brazil. j_eduardo_lira@yahoo.com.br*
[2] *Physics Department, M-OSRP, University of Houston, Houston, TX 77204-5005, U.S.A. aweglein@central.uh.edu*
[3] *University of Calgary, CREWES Project, Dept. of Geoscience, Calgary, AB, Canada T2N 1N4. k.innanen@ucalgary.ca*
[*] *Present address: ConocoPhillips Canada, 401-9th Avenue S.W., Calgary, AB, Canada T2P 2H7. Chris.W.Bird@conocophillips.com*

(Received January 24, 2012; revised version accepted September 18, 2012)

ABSTRACT

Lira, J.E., Weglein, A.B., Bird, C.W. and Innanen, K.A., 2012. Determination of reflection coefficients by comparison of direct and reflected VSP events. *Journal of Seismic Exploration*, 21: 361-376.

VSP experiments provide a much greater opportunity to estimate local reflectivity information than do surface-constrained experiments. In this paper we describe a simple, data driven means by which the reflection coefficient associated with an interface at depth, uncontaminated by transmission losses, may be determined, regardless of the origins of these losses or of the overburden parameters associated with them. An amplitude correction operator is formed through a comparison of the direct and reflected waves just above a generating interface. Error grows as the distance above the generating interface at which the two events are compared grows. The formulation of the problem is in the plane-wave domain, but with a slight additional error the approach can be applied to data associated with fixed zero or nonzero offset. The method can be applied to generate scalar reflectivity values in acoustic/elastic environments, or phase and amplitude spectra of reflectivities in anacoustic/attenuative environments. A field data example from the Ross Lake heavy oil field in Saskatchewan, Canada illustrates the method. Our sense is that these results indicate applicability to more complex geometries, walkway or 3D VSP surveys, assisting with the construction of AVO/AVA panels.

KEY WORDS: VSP, absorption, amplitudes, frequency domain, reflection coefficients, borehole geophysics.

0963-0651/12/$5.00 

## INTRODUCTION

VSP has become an increasingly important tool for oil exploration during the last two decades. In that time, the development of computational and instrument technology, along with an increased need to understand and monitor production of existing reservoirs, has led to an evolution of the VSP method from 1D time-only measurements to far more complex multi-D geometries. The first 3D VSP, for instance, was acquired by AGIP in 1986 (Chopra et al., 2004), and since then 3D has become an affordable and viable option for monitoring production (Kuzmiski et al., 2009). For an early historical review see Hardage (1985). VSPs are used for anisotropic parameter estimation (Grechka and Mateeva, 2007), attenuation studies (Omnes and Heprenschmidt, 1992), anisotropic AVO analysis (Leaney et al., 1999), stiffness tensor calculation (Dewangan and Grechka, 2002), mapping of fluid pathways (Owusu and Mubarak, 2009), etc.

As in surface seismic exploration, the need for *a priori* earth property information is characteristic of conventional VSP processing. In the surface case, the attempt to reduce this need has met with remarkable success, in, e.g., free-surface multiple elimination (Carvalho, 1992; Verschuur et al., 1992), internal multiple attenuation (Araujo et al., 1994; Ramirez, 2007), and is the subject of more recent advances in imaging (Weglein et al., 2012). The literature contains a shorter record of this kind of progress for the VSP problem, yet the interest exists there too: Xiao et al. (2006) and He et al. (2009), for instance, present VSP imaging approaches that avoid the requirement for prior knowledge of medium properties. In this paper we consider a related problem: determining the reflection coefficients associated with structures in a VSP experiment directly from the amplitudes of the VSP data, which contain the reflectivity but are also influenced by overburden transmission of various kinds.

The approach we take is based on a simple picture of the origins of the amplitude of a reflected primary. This amplitude, say P, is represented as involving the influence of propagation down through the overburden, $P_D$, reflection at an interface, R, followed by propagation back up through some or all of the overburden, $P_U$. The amplitude is thus the cumulative effect of three influences:

$$P = P_D R P_U \quad . \tag{1}$$

The success of most VSP data processing and/or imaging problems is connected to the ability to identify and remove the influence of $P_D$ and $P_U$, recovering the reflectivity information R.

Our approach involves a compensation procedure, in which we correct P for its transmission losses, by designing an operator (a "primary correction

operator", or PCO for short) directly from the raw VSP data (i.e., directly from the shot records), {without using} medium property information. The operator, which is effectively of the form PCO = $1/\{[P_D][P_U]\}$, is constructed through a combination of the amplitude spectra of the primary and its direct wave counterpart, each recorded at the same receiver. A related combination of direct and transmitted waves is discussed by Hardage (1985). Its precise form is deduced, in this paper, from a study of the direct and reflected amplitude spectra for earths of two distinct types, acoustic and anelastic.

We illustrate its use with simple numerical examples for a zero-offset VSP. We emphasize, however, that the approach with which data from one or more non-zero offsets is processed is unchanged. We discuss the gradual increase in correction error with increase in offset in an upcoming section.

## VSP MODELS AND CONFIGURATION

We consider a VSP experiment with a zero offset (Fig. 1). We assume, first, layered acoustic media, and second, layered anacoustic media (i.e., involving attenuation and dispersion). The n-th layer lies between the n-th and the (n+1)-th interface. These choices are made to exemplify the procedure, which is not constrained to media of these types, but is essentially independent of model-type.

### Case I: R beneath an acoustic overburden

We begin by deducing the form of the primary amplitude correction operator PCO for an acoustic, one-parameter overburden, pictured in the left-hand panel of Fig. 1. Suppose the direct wave and the primary reflecting from interface n are both measured by a geophone at depth z (Fig. 2). In one spatial dimension, the phase and amplitude of the primary are constructed as follows:

$$P = e^{ik_0(z_1-z_0)}\, T_{01} e^{ik_1(z_2-z_1)}\, T_{12} e^{ik_2(z_3-z_2)} \ldots$$

$$\times\, R_n \exp[ik_{n-1}(2z_n - z_{n-1} - z)] \quad , \tag{2}$$

such that

$$|P| = [T_{01}T_{12}T_{23} \ldots T_{(n-1)n}] \times R_n \quad , \tag{3}$$

where $z_n$ is the depth of the n-th interface, $k_n = \omega/c_n$, $c_n$ is the wave velocity in the n-th layer, $\omega$ is the frequency, and $T_{ij}$ is the transmission coefficient at the interface between layers i and j.

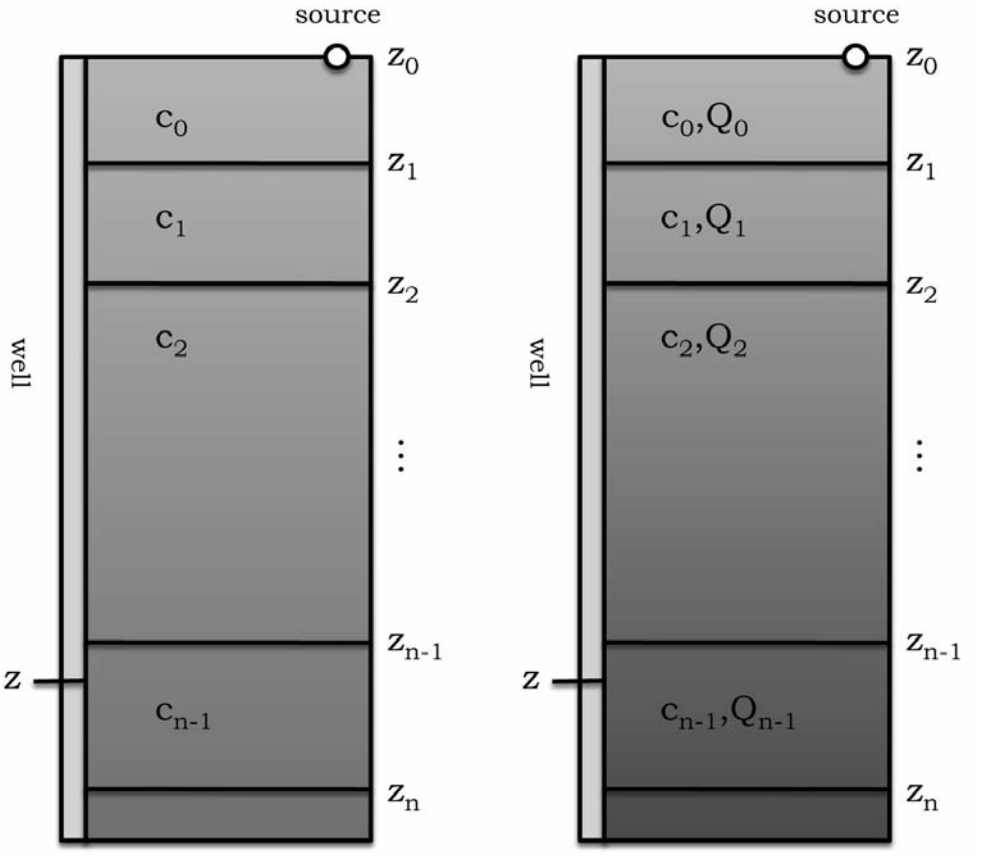


Fig. 1. 1D zero-offset VSP geometry and parameters. Left: one-parameter acoustic model. Right: two-parameter anacoustic (i.e., attenuative and dispersive) model.

The phase and amplitude of the direct wave are likewise constructed via

$$D = e^{ik_0(z_1-z_0)}T_{01}e^{ik_1(z_2-z_1)}T_{12}e^{ik_2(z_3-z_2)}\ldots \times \exp[ik_{n-1}(z - z_{n-1})] \ , \tag{4}$$

such that

$$|D| = [T_{01}T_{12}T_{23}\ldots T_{(n-1)n}] \ . \tag{5}$$

Evidently, the reciprocal of the direct wave spectrum in eq. (5) must be the desired operator (PCO) described above, which, when applied to the primary spectrum, corrects for the transmission losses:

$$\begin{aligned} P_{cor} &= |P| \times PCO = |P| \times 1/|D| \\ &= [T_{01}T_{12}T_{23} \ldots T_{(n-1)n}] \times R_n \times 1/[T_{01}T_{12}T_{23} \ldots T_{(n-1)n}] \\ &= R_n \ . \end{aligned} \tag{6}$$

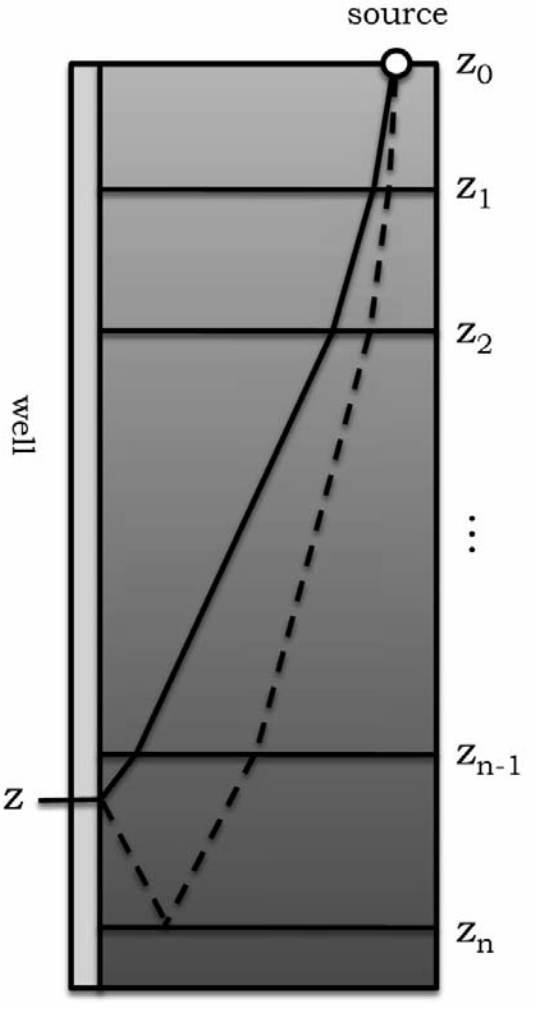


Fig. 2. 1D zero-offset VSP survey. The direct wave (solid) and the primary $P_n$, generated at interface n (dashed), are depicted. The two paths are identical except for (1) small differences in path length due to (very small) offset, and (2) a small additional path segment experienced by the primary below z.

This 1D model of amplitudes is correctly understood as applying to a plane wave, in which domain eq. (6) can be applied at normal or oblique incidence. However, since in a VSP experiment we rarely have sufficient spatial source coverage to permit Fourier transformation to the plane-wave domain, we will analyze this formula as applied in the spatial domain, that is, involving data from fixed zero or non-zero offsets.

In the fixed offset case several aspects of the model in eqs. (2) - (6) are inaccurate - for instance no account of spherical spreading has been taken. We point out, however, that since two events with nearly identical paths of propagation are being compared, and all amplitude influences shared by the two events are "divided out", the additional error introduced by applying a correction based on this model to fixed offset VSP data should be relatively small.

## Case II: R(ω) beneath an attenuating overburden

To study the attenuative case, in which transmission losses are magnified considerably, we adopt the model reviewed by Aki and Richards (2002), wherein the acoustic propagation constants $k_j$ in eq. (2) is replaced by the complex $k_j^*$, such that for the j-th layer

$$k_j^* = (\omega/c_j)[1 + (1/Q_j)F(\omega)] \quad , \tag{7}$$

where

$$F(\omega) = (i/2) - (1/\pi)\log(\omega/\omega_0) \quad , \tag{8}$$

and $\omega_0$ is a reference frequency. Substituting $k_j^*$ for $k_j$ in eq. (2) and re-grouping the terms, we express the anelastic primary as:

$$P_{an} = e^{ik_0^*(z_1-z_0)}\, T_{01} e^{ik_1^*(z_2-z_1)}\, T_{12} e^{ik_2^*(z_3-z_2)} \ldots$$
$$\times R_n(\omega)\exp[ik_{n-1}^*(2z_n - z_{n-1} - z)] \quad , \tag{9}$$

where the absorptive transmission coefficients $T_{ij}$ are defined as follows:

$$T_{ij} = [2c_j(1+F(\omega)/Q_j)^{-1}/\{c_i(1+F(\omega)/Q_i)^{-1} + c_j(1+F(\omega)/Q_j)^{-1}\}]$$
$$\times \underbrace{e^{-(\omega/2Q_ic_i)(z_i-z_{i-1})}}_{\text{attenuation component}}\, e^{(i\omega/\pi Q_ic_i)\log(\omega/\omega_0)(z_i-z_{i-1})} \quad , \tag{10}$$

as discussed by Lira et al. (2010). We re-write the direct wave in analogy to

eq. (4):

$$D_{an} = e^{ik_0^*(z_1-z_0)}\, T_{01} e^{ik_1^*(z_2-z_1)}\, T_{12} e^{ik_2^*(z_3-z_2)} \ldots$$

$$\times \exp[ik_{n-1}^*(z - z_{n-1})] \quad . \tag{11}$$

Eqs. (9) and (11) are to the anelastic case what eqs. (2) and (4) are to the acoustic case, hence we repeat the procedure and define an absorptive operator $PCO_{an}$, which, when applied to the spectrum of the primary produces:

$$PCO_{an} \times P_{an} = (1/D_{an}) \times P_{an} = R_n(\omega) \times e^{ik_{n-1}^* 2(z_n - z)} \quad . \tag{12}$$

Neglecting the (small) term $e^{ik_{n-1}^* 2(z_n - z)}$ in eq. (12), we again have generated the correction operator. In comparing the acoustic and attenuative cases, the only difference is that we have retained the phase content of the reflections in the latter. In spite of this slight implementation difference, the operator is designed the same way independent of the mechanism of transmission loss in the overburden: no matter what type of medium is assumed, the correction is carried out the same way.

## SOURCES OF ERROR

There are two main sources of error in the operator design as we have presented it. One source of error is visible in the construction of the operators. Consider again eq. (12). The extra factor,

$$\exp[ik_{n-1}^* 2(z_n - z)] \quad , \tag{13}$$

being extraneous, slightly throws the calculation off. The origin of this term lies in the fact that we must compare the direct wave and primary some small but finite distance above the generating reflector. This adds a short component to the primary's path not shared by the direct wave (see Fig. 2). The error is kept small provided the distance from the generating interface to the receiver is relatively small. In this case

$$|ik_{n-1}^* 2(z_n - z)| \ll 1 \quad , \tag{14}$$

and

$$PCO_{an} \times P_{an} \rightarrow R_n(\omega) \quad . \tag{15}$$

Beyond this source of error, the diagram in Fig. 2 also illustrates the influence of offset on the accuracy of the operator construction. Briefly, the greater the offset, the longer the path of the primary *not* shared by the direct wave must be. This effectively increases the importance of the extra term [eq. (13)].

## SYNTHETIC EXAMPLES

Here we illustrate with synthetic examples the transmission loss compensation in action on a 1D zero-offset VSP experiment in an absorptive medium as mathematically modeled in the previous section. We generate three zero-offset traces from plane-waves incident normally upon the model depicted in the right-hand panel of Fig. 1. We use parameter values given in Table 1.

Table 1. Attenuative earth models. The columns labelled $M_1$, $M_2$ and $M_3$ contain the layer Q values for models 1, 2 and 3, respectively.

| Layer | Depth (m) | c (m/s) | $M_1$ | $M_2$ | $M_3$ |
|---|---|---|---|---|---|
| 0 | 0-100 | 1500 | $\infty$ | $\infty$ | $\infty$ |
| 1 | 100-350 | 1700 | 400 | 300 | 100 |
| 2 | 350-600 | 1800 | 200 | 150 | 50 |
| 3 | 600-850 | 1950 | 100 | 75 | 25 |
| 4 | 850-1100 | 2000 | 50 | 25 | 15 |
| 5 | 1100-$\infty$ | 2100 | 25 | 15 | 10 |

In Fig. 3 the three input traces are illustrated. The Q values used for each trace range from low to high attenuation. Our goal is to correct the amplitude of the primary using the direct wave. The procedure is: (1) the primary and its {direct wave} counterpart, at the same receiver, are isolated and their spectra calculated, (2) the reciprocal of the spectrum of the direct wave, which is identified as the operator PCO, is taken, and (3) the spectrum of the primary is multiplied by the operator. The reciprocal spectra, i.e, the PCOs, are displayed in Fig. 4. Fig. 5 compares the original primary with the corrected primary and both vs. the idealized case (modeled with no transmission losses) which serves as a benchmark.

Comparing the latter two traces, we observe that the overburden transmission losses are largely compensated for, with some small visible error attributable to the distance above the reflector at which the analysis is conducted.

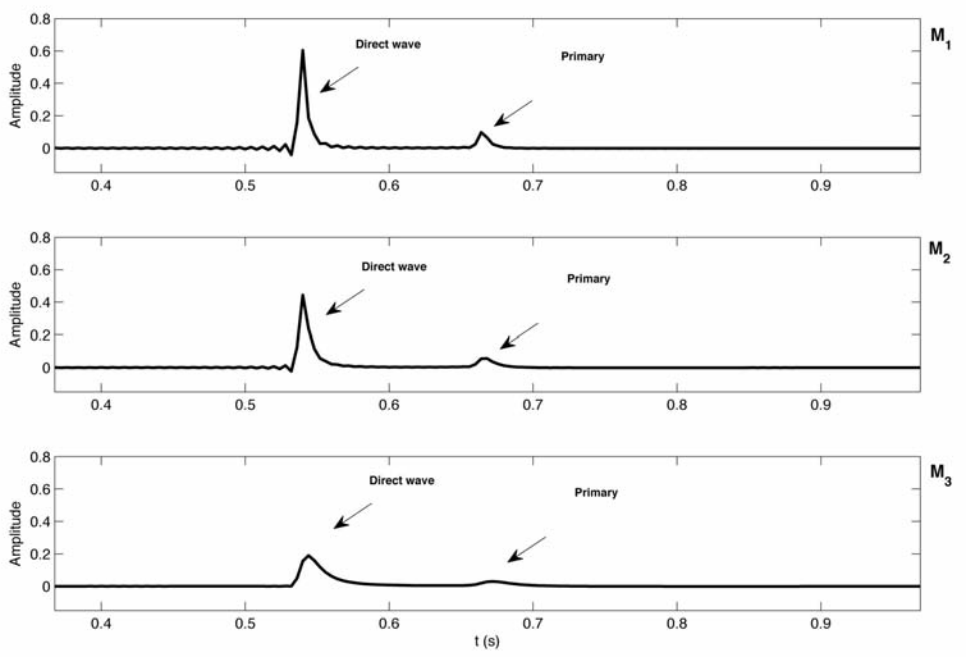


Fig. 3. Three zero-offset traces generated with the survey geometry depicted in (a), using parameters in Table 1. Two events are shown: the direct wave and the primary.

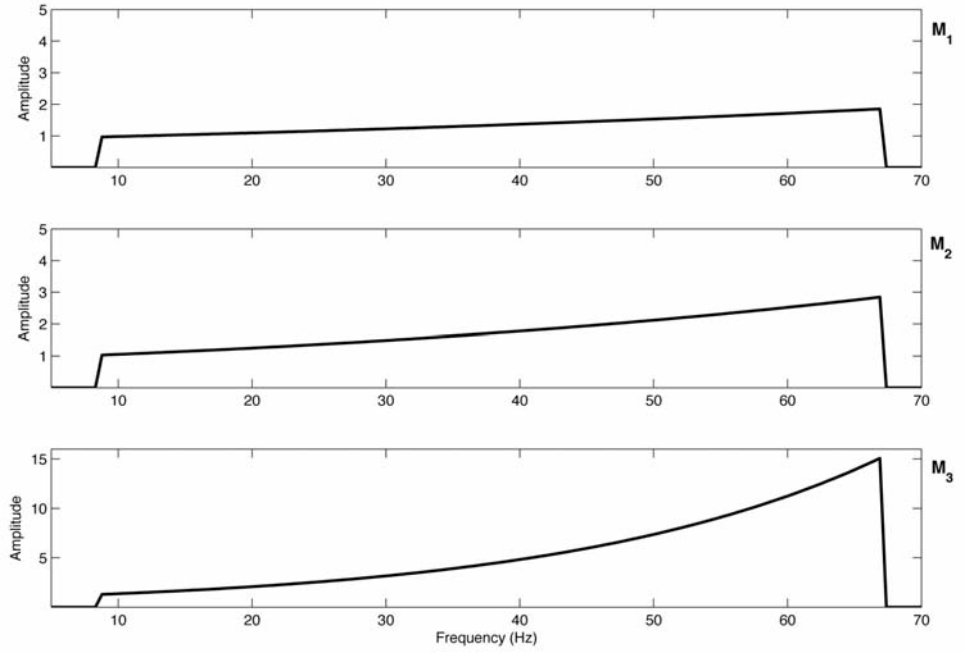


Fig. 4. Illustration of the three PCO spectra calculated from the direct waves illusrated in Fig. 2.

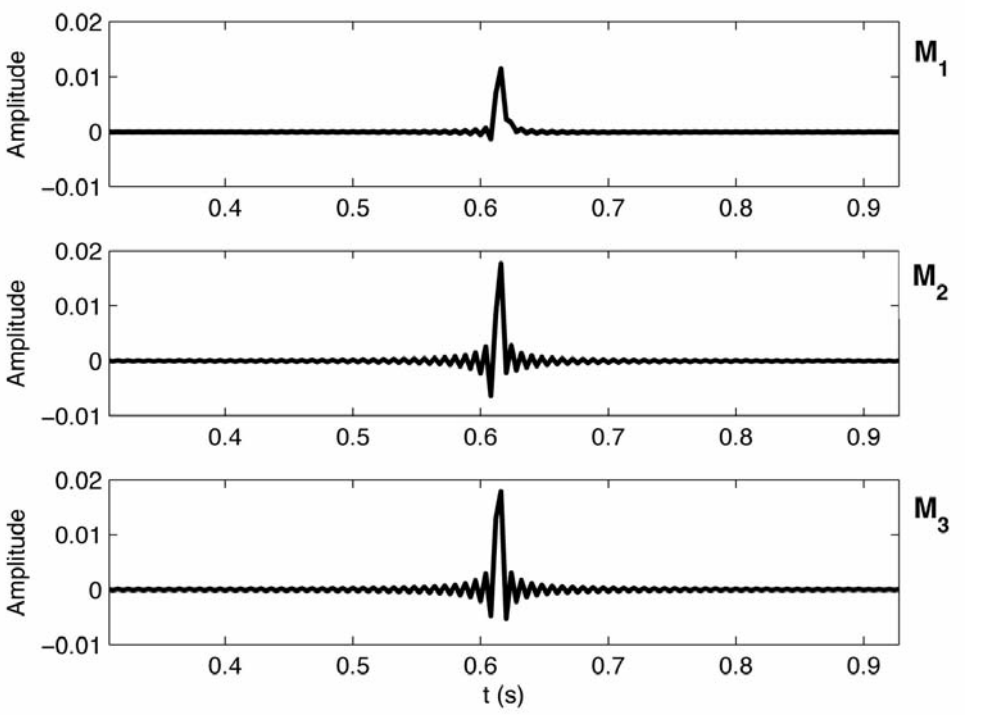


Fig. 5. Result of correction of primary $M_2$. Top panel: input; middle panel: corrected with the PCO. Bottom panel: benchmark: primary modeled in the absence of transmission influences.

## FIELD DATA EXAMPLE: ROSS LAKE

The Ross Lake heavy oil field is located in the southwest of Saskatchewan (see Fig. 6), and is owned and operated by Husky Energy Inc. (Zhang, 2010). In a collaboration between CREWES/University of Calgary, Husky Energy, and Schlumberger Canada, a number of VSP experiments were {performed including a zero-offset VSP}.

The zero-offset VSP will be the focus of this paper. The data were acquired using 3-component receivers and both horizontal and vertical vibrators (Zhang, 2010). The receiver spacing in the borehole was 7.5 m. There is a reflector at roughly 600 m depth which is likely associated with the Lea Park/Milk river unconformity. In Fig. 7 for the stratigraphic column is illustrated.


Fig. 6. Ross Lake oil field in Saskatchewan. From Zhang (2010).

In Figs. 9 and 10 the vertical component of the downgoing and upgoing wave fields are plotted, respectively. Wave field separation was performed using a median filtering technique (Kommedal and Tjostheim, 1989; Hinds et al., 1996). Fig. 10 shows the aforementioned reflection at 600 m which has been interpreted and is highlighted in orange.

A $Q_P$ profile was obtained by Zhang (2010) using the spectral shift method (e.g., Hauge, 1981) on the VSP data to obtain a profile of $Q_P$ in the vicinity of the wellbore. This $Q_P$ profile is on the far left panel of Fig. 8. Importantly for our current purposes, there is a negligible attenuation contrast at the Lea Park/Milk River interface. Therefore, we expect that there should be little frequency dependence of the reflection coefficient and we may use the ratio of the peak amplitudes to provide the estimate of the reflection coefficient.

We extract the amplitudes of the interpreted direct arrival on the downgoing wavefield dataset, then we extract the amplitude of the interpreted Lea Park/Milk River horizon on the upgoing wavefield dataset.

We then divide the reflected amplitudes by the direct arrival amplitudes for each receiver to obtain an estimate of the reflection coefficient. For receivers

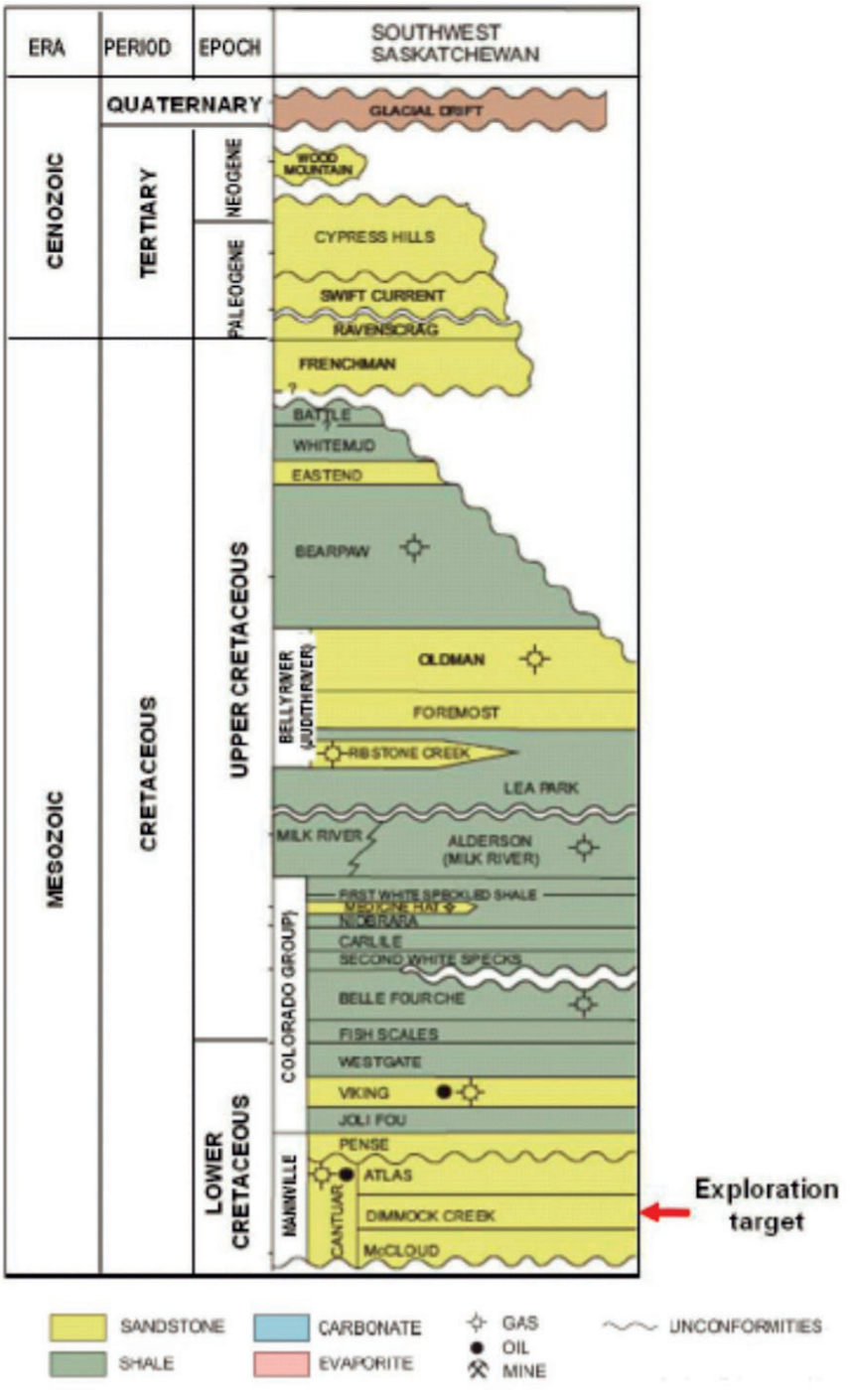


Fig. 7. Stratigraphic column of study area. From Saskatchewan Industry and Resources, 2006; adapted from Zhang (2010).

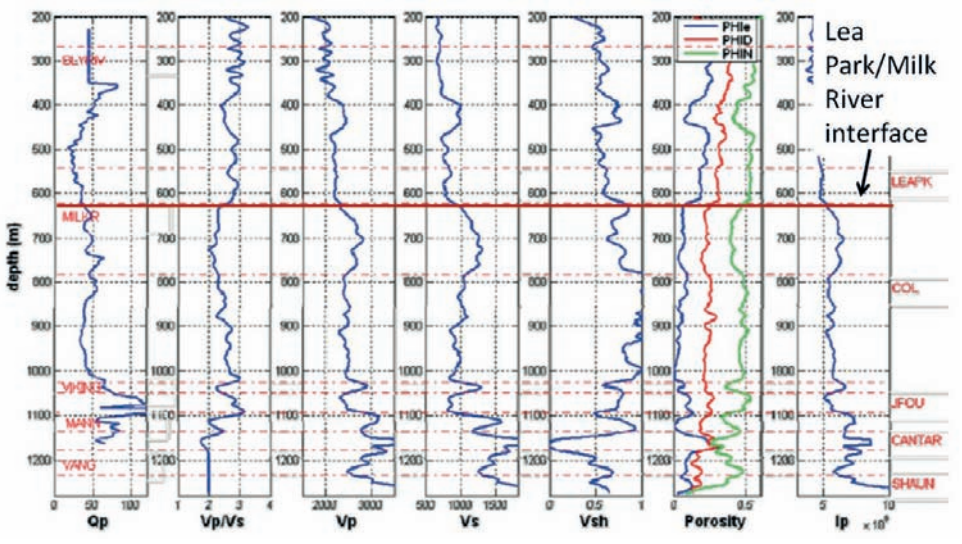


Fig. 8. Left column: $Q_P$ profile using spectral shift method. From Zhang (2010).

just above the reflector the result of dividing the reflected amplitude from the direct amplitude should be a close approximation to the reflection coefficient. However, as we move up the borehole the extracted amplitudes of the primary will decay due to the propagation effect of the attenuative medium and so the estimate of the reflection coefficient obtained by dividing the reflected amplitude by the direct amplitude should be less than the correct reflection coefficient.

Fig. 11 shows a plot of the estimated reflection coefficient versus the distance of the receiver above the reflector from which the estimate was obtained. The blue curve shows the actual values of the reflection coefficient and the red curve is a line of best fit. Notice that the reflection coefficient drops as the distance above the reflector increases, as expected. The best estimate of the reflection coefficient in Fig. 11 will be where the receiver is closest to the reflector which is about 0.08.

## CONCLUSIONS

We discuss a strategy for correcting the transmission losses of a primary using an operator built from data only. The operator is calculated with no *a priori* earth property information, and the procedure is identical no matter what type of medium, or mechanism of transmission loss, is present, and the correction is achieved in principle directly from shot records.

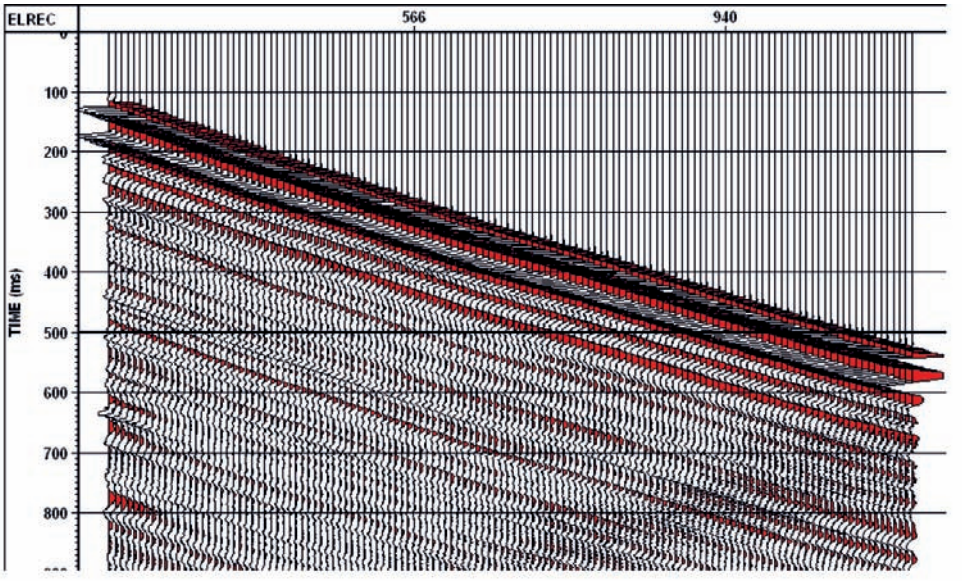


Fig. 9. The downgoing wavefield, separated using median filtering.

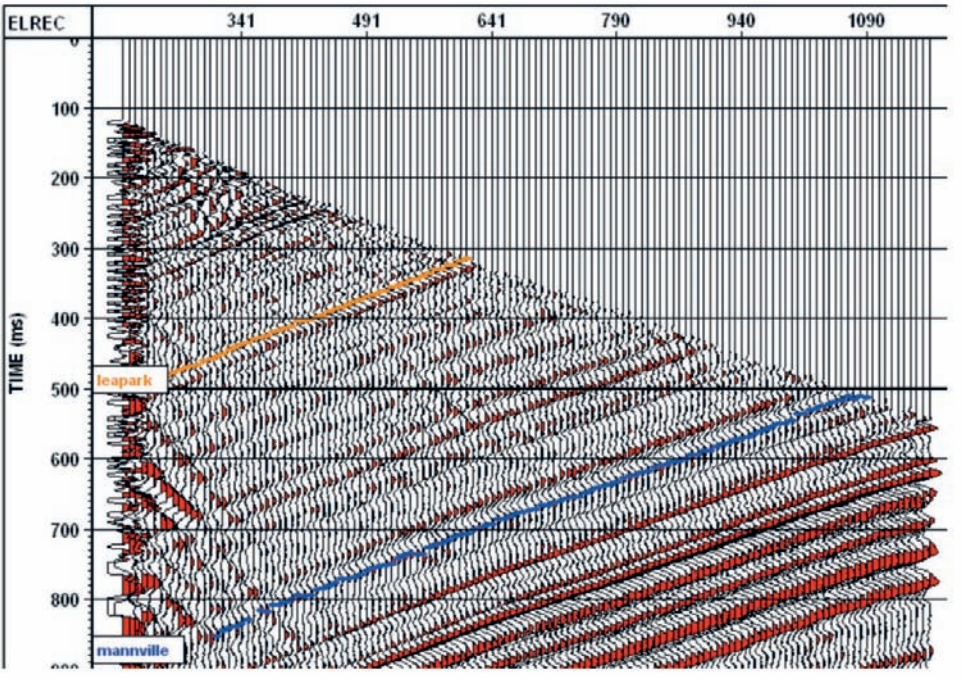


Fig. 10. The upgoing wavefield, separated using median filtering, with the Lea Park and Mannville horizons interpreted.

We illustrate three zero-offset synthetic examples involving low and high levels of overburden attenuation. The results of the numerical study have been sufficiently encouraging to warrant field data testing.

We apply the approach to field data from the Ross Lake oil field in southwest Saskatchewan, obtaining a reasonable result for a reflection coefficient for the Lea Park/Milk River reflector. This result will need to be verified with well log data.

Our sense is that these results indicate applicability to more complex geometries, walkway or 3D VSP surveys, assisting with the construction of AVO/AVA panels. These panels could be produced, in principle, as the shots are being recorded at the time of acquisition.

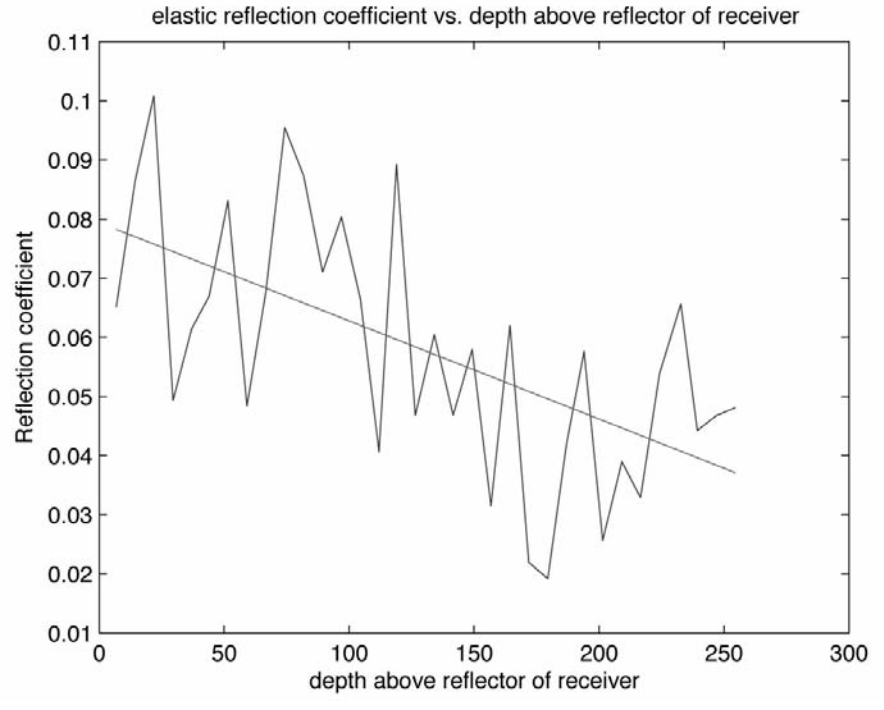


Fig. 11. Estimate of the reflection coefficient as a function of receiver distance above the reflector.

## ACKNOWLEDGMENTS

J. Lira thanks Petrobras. A.B. Weglein thanks the sponsors of M-OSRP. C. Bird and K. Innanen thank the CREWES Project, and are additionally supported by an NSERC Discovery grant. The Ross Lake VSP data set was acquired in 2003 by the CREWES Project, Husky Energy Inc., and Schlumberger Canada.

## REFERENCES

Aki, K. and Richards, P.G., 2002. Quantitative Seismology, 2nd Ed. University Science Books, Sausalito, California.

Araujo, F.V., Weglein, A.B., Carvalho, P.M. and Stolt, R.H., 1994. Inverse scattering series for multiple attenuation: An example with surface and internal multiples. Expanded Abstr., 64th Ann. Internat. SEG Mtg., Los Angeles: 1039-1041.

Carvalho, P.M., 1992. Free-surface Multiple Reflection Elimination Method Based on Non-linear Inversion of Seismic Data. Ph.D. Thesis, Universidade Federal da Bahia, Bahia, Brazil.

Chopra, S., Alexeev, V., Manerikar, A. and Kryzan, A., 2004. Acquisitions/Processing Processing/Integration of simultaneously acquired 3D surface seismic and 3D VSP data. The Leading Edge, 23: 422-430.

Dewangan, P. and Grechka, V., 2002. Inversion of multicomponent, multiazimuth, walkaway VSP data for the stiffness tensor. Expanded Abstr., 72nd Ann. Internat. SEG Mtg., Salt Lake City: 161-164.

Grechka, V. and Mateeva, A., 2007. Inversion of P-wave VSP data for local anisotropy: Theory and case study. Geophysics, 72: D69-D79.

Hardage, B.A., 1985. Vertical Seismic Profiling, Part A: Principles, 2nd Ed. Geophysical Press, Ltd., London.

Hauge, P.S., 1981. Measurements of attenuation from vertical seismic profiles. Geophysics, 46: 1548-1558.

He, R., Karrenbach, M., Paulsson, B. and Soutryne, V., 2009. Near-wellbore VSP imaging without overburden. Geophysics, 74: SI9-SI14.

Hinds, R.C., Anderson, N.L. and Kuzmiski, R.D., 1996. VSP Interpretive Processing: Theory and Practice. SEG, Tulsa, OK.

Kommedal, J.H. and Tjostheim, B.A., 1989. A study of different methods of wavefield separation for application to VSP data. Geophys. Prosp., 37: 117-142.

Kuzmiski, R., Charters, B. and Galbraith, M., 2009. Processing considerations for 3D VSP. Recorder, 34: 30-40.

Leaney, W.S., Sayers, C.M. and Miller, D.E., 1999. Analysis of multiazimuthal VSP data for anisotropy and AVO. Geophysics, 64: 1172-1180.

Lira, J.E.M., Innanen, K.A., Weglein, A.B. and Ramirez, A.C., 2010. Correction of primary amplitudes for plane-wave transmission loss through an acoustic or absorptive overburden with the inverse scattering series internal multiple attenuation algorithm: an initial study and 1D numerical examples. J. Seismic Explor., 19: 19-34.

Omnes, G. and Heprenschmidt, A., 1992. Use of VSP data for P- and S-wave attenuation studies in a fractured reservoir. Expanded Abstr., 62nd Ann. Internat. SEG Mtg., New Orleans: 148-150.

Owusu, J.C. and Mubarak, M., 2009. High-fidelity walkaround VSP anisotropy analysis. The Leading Edge, 28: 966-972.

Ramirez, A.C., 2007. I - Inverse scattering subseries for 1: Removal of internal multiples and 2: Depth imaging primaries; II - Green's theorem as the foundation of interferometry and guiding new practical methods and applications. Ph.D. Thesis, University of Houston.

Verschuur, D.J., Berkhout, A.J. and Wapenaar, C.P.A., 1992. Adaptive surface-related multiple elimination. Geophysics, 57: 1166-1177.

Weglein, A.B., Liu, F., Li, X., Terenghi, P., Kragh, E., Mayhan, J.D., Wang, Z., Mispel, J., Amundsen, L., Liang, H., Tang, L. and Hsu, S.-Y., 2012. Inverse scattering series direct depth imaging without the velocity model: first field data examples. J. Seismic Explor., 21: 1-28.

Xiao, X., Zhou, M. and Schuster, G.T., 2006. Salt-flank delineation by interferometric imaging of transmitted P- to S-waves. Geophysics, 71: SI197-SI207.

Zhang, Z., 2010. Assessing attenuation, fractures, and anisotropy using logs, vertical seismic profile, and three-component seismic data: heavy oilfield and potash mining examples. Ph.D. Thesis, University of Calgary, Alberta.